INTERNATIONAL SOCIETY FOR SOIL MECHANICS AND GEOTECHNICAL ENGINEERING

This paper was downloaded from the Online Library of the International Society for Soil Mechanics and Geotechnical Engineering (ISSMGE). The library is available here:

https://www.issmge.org/publications/online-library

This is an open-access database that archives thousands of papers published under the Auspices of the ISSMGE and maintained by the Innovation and Development Committee of ISSMGE.

The paper was published in the proceedings of the 10th European Conference on Numerical Methods in Geotechnical Engineering and was edited by Lidija Zdravkovic, Stavroula Kontoe, Aikaterini Tsiampousi and David Taborda. The conference was held from June 26th to June 28th 2023 at the Imperial College London, United Kingdom.

To see the complete list of papers in the proceedings visit the link below:

https://issmge.org/files/NUMGE2023-Preface.pdf

Proceedings 10th NUMGE 2023
10th European Conference on Numerical Methods in Geotechnical Engineering
Zdravkovic L, Kontoe S, Taborda DMG, Tsiampousi A (eds)

© Authors: All rights reserved, 2023
https://doi.org/10.53243/NUMGE2023-227

Is the maximum shear stress, in an assumed constant shear drained stress path, really constant?

D. Reid[1] , R. Fanni[1,2] , A. Fourie[1]

[1]*Department of Civil, Environmental and Mining Engineering, The University of Western Australia, Perth, Australia*

[2]*WSP Golder, Perth, Australia*

ABSTRACT: The constant shear drained (CSD) stress path has received significant attention over the past few decades and is recognised as one of the most common, and potentially dangerous stress paths that can lead to static liquefaction triggering. The primary means through which the CSD stress path has been investigated is stress controlled triaxial element tests, with some recent works also utilising plane strain, direct simple shear, and hollow cylinder torsional shear (HCTS) devices. A common assumption when carrying out CSD tests is that below a slope with a rising phreatic surface, deviator stress will remain constant. However, this assumption has not been adequately tested. For example, the limited plane strain testing available appears to suggest that deviator stress and Lode Angle will vary. Alternatively, triaxial and HCTS tests used to study this stress path usually maintain a constant deviator stress. This paper examines the stress conditions under a rising phreatic surface using an idealised embankment geometry, with the NorSand constitutive model adopted for the analyses. The stress paths seen in the simplified boundary element problem vary, with some decrease in deviator stress at some locations, helping to inform future experimental designs to study the CSD (or similar) stress paths.

Keywords: Static liquefaction; constant shear drained; slope stability

1 INTRODUCTION

The initiation of instability from a rising phreatic surface represents an important trigger mechanism for earth structures comprising loose saturated soil. This stress path is commonly referred to as the constant shear drained (CSD) stress path (Anderson and Riemer 1995). As implied by the name, the CSD stress path idealisation is that below a slope, the shear stresses will remain relatively consistent owing to an unchanging slope geometry – indeed, this has been the idealisation assumed since first discussed (e.g. Brand 1985). The stress path is referred to as being drained as it is common for an increase in the phreatic surface within slopes to occur at such a rate that – at least initially, prior to instability – free drainage of all elements below the slope is maintained. Thus, the stress ratio $\eta = q/p'$ increases owing to a decrease in p' while q is viewed as remaining constant.

There are a few potential complications to the constant shear stress idealisation. For example, an increase in phreatic surface would lead to a higher degree of saturation in the slope, thus increasing bulk density, and potentially the shear stress acting on elements of soil further upstream. Further, there is evidence from plane strain tests (Wanatowski 2005, Wanatowski et al. 2010) that the unloading process may lead to changes to intermediate principal stress ratio b (Bishop 1966) and the magnitude of q in some cases. Finally, the authors are unaware of any published examples of the CSD stress path that examine this issue in detail in a boundary value problem (BVP).

Owing to the importance of the CSD stress path on the stability of tailings deposits and earth structures comprising loose saturated soils and the sparse information as to how in situ stress conditions would evolve on this stress path in a BVP, this paper outlines analysis of an idealised slope under a rising phreatic surface. The evolution of stress conditions as predicted by the NorSand constitutive model (Jefferies 1993) are tracked at six points below the slope to allow the examination.

2 LABORATORY TESTING REVIEW

As with soil testing more generally, laboratory element studies of the CSD stress path are dominated by the triaxial compression test. However, some variation has been seen more recently, which has allowed expansion of the understanding of the mechanism and comparison of the triggering of instability on a CSD path to conventional undrained shearing. A summary of laboratory investigations of the CSD path are summarised as follows:

Triaxial compression: The seminal first demonstration of the potential for static liquefaction triggering on a CSD path was made by Sasitharan et al. (1993) where q was applied, and maintained at a near-constant value by dead weights. This work was expanded by Skopek et al (1994) who, using dry specimens with internal instrumentation, was able to link the initiation of rapid contraction after a sufficient increase in η to the collapse seen in the work of Sasitharan et al. Subsequently, a range of test programs on a wide range of densities to enable developed of instability stress ratio η_{IL} vs density/state parameter (Ψ) relationships (di Prisco and Imposimato 1997, Gajo et al. 2000, Chu et al. 2003). Importantly, all the triaxial compression studies attempted - where possible, owing to the loading rates of the various devices used and/or the inclusion of area correction effects - to maintain q, consistent with a constant shear stress idealisation.

Triaxial extension: Dong et al. (2016) carried out CSD tests under triaxial extension conditions, again maintaining a constant q. Much lower values of η_{IL} were observed compared to triaxial compression, consistent more generally with the anisotropic behaviour of loose sands.

Plane strain compression: Wanatowski et al.(2010) carried out CSD tests in a purpose-built plane strain device. The CSD stress path involved maintenance of a constant major/minor principal stress difference σ_1- σ_3, with the evolution of the intermediate principal effective stress σ'_2 tracked by means of pressure cells. Lower values of η_{IL} were seen in the plane strain tests consistent with a decreased critical state friction ratio M under the prevailing conditions b in the tests. Importantly, b was seen to increase as the CSD stress path proceeded, a useful observation not possible in previous laboratory test programs of the CSD stress path.

SGI-type direct simple shear (DSS): Reid and Fourie (2019) used a modified SGI-type DSS to carry out CSD tests. A constant τ_{vh} was applied with dead weights, with this being the only option in an SGI-type DSS. Like triaxial compression and extensions tests, instability at η values far lower than critical were seen.

Hollow cylinder torsional shear (HCTS) system: Fanni et al. (2022) carried out CSD tests in an HCTS under a range of principal stress angle α and b values to investigate the effects of general stress conditions on the initiation of instability. Consistent with expectations (e.g. Reid 2020) and trends for undrained shearing, η_{IL} for triggering decreased with increasing principal stress angle. A constant q value was applied during the CSD path.

While many laboratory examinations of the CSD stress path have been carried out, only the program of Wanatowski et al. (2010) was under plane strain conditions somewhat representative of conditions below an infinite slope. However, this test features vertical α and required the assumption of a constant σ_1- σ_3 difference during the test. It is unclear whether this is a reasonable assumption for the evolution of stresses below a slope with a rising phreatic surface. Given the clear importance of studying generalised stress conditions on CSD triggering (Fanni et al. 2022), additional information as to the likely behaviour below slopes under these conditions would be useful. An idealised embankment geometry is therefore used to study the stress paths followed in a rising phreatic surface.

3 CONSTITUTIVE MODEL AND PARAMETERS

Prior to development of a BVP, selection and calibration of a constitutive model is first required. Given the ubiquity of critical state soil mechanics (CSSM)-based techniques to current tailings engineering practice a model based on CSSM was desired. At an element-level, the authors are aware of three CSSM-based constitutive models that have produced reasonable representations of the CSD stress path: (i) NorSand - when including the inner cap (Jefferies 1997, Jefferies and Been 2015) to allow plastic unloading, (ii) a modified version (Alipour and Lashkari 2018) of the Sanisand model, (iii) and the Severn-Trent model (Gajo and Wood 1999, Gajo 2004). The authors adopted the NorSand model in the current work owing to its ubiquity in tailings engineering practice and its implementation – with inner cap – in some commercially-available numerical codes.

To produce a calibrated model of NorSand for a soil with both CSD tests and sufficient data for calibration purposes, the Silica Fine sand (SFS) tested by Fanni et al. (2022) was selected. Interrogation of this data led to the calibration outlined in Table 1. Of particular importance for the modelling of the CSD stress path is the state dilatancy constant χ, which controls the location of the NorSand inner cap. The initial selection of χ presented in Table 1 was based on a series of dense drained tests on SFS, consistent with conventional practice (Jefferies and Been 2015). Elastic shear modulus G is based, for initial calibration checks, on bender element tests presented by Chow et al. (2019) – i.e. G_{max}.

Table 1. NorSand parameters developed for SFS

Parameter	Description	Unit	Value
Γ	CSL intercept	-	0.761
λ_e	CSL slope	-	0.008
M_{tc}	Critical state friction ratio	-	1.24
χ	State dilatancy	-	3.1
N	Volumetric coupling parameter	-	0.25
H	Plastic hardening	-	=70-560Ψ
G	Elasticity	MPa	$=50(p'/p_{atm})^{0.5}$
ν	Poisson's ratio	-	0.20

While not relevance to element simulations, it is noted that in the subsequent application of the SFS calibration of NorSand to a BVP problem, a dry density of 1.7 t/m^3 and porosity of 0.3 were used.

Element CSD simulations were first carried out using the SFS parameters outlined in Table 1, to simulate the loose triaxial compression test 6-TX3 carried out by Fanni et al. (2022). It was immediately evident that the inner cap location suggested from state-dilatancy interpretation of dense drained triaxial compression tests did not appear to well represent the initiation of plastic yielding unloading for the available CSD tests. Therefore, χ was iteratively adjusted until the simulation produced contraction towards the CSL in a reasonably similar pattern to the experimental observations, which required $\chi = 10.5$. This calibration is presented in a state diagram in Figure 1.

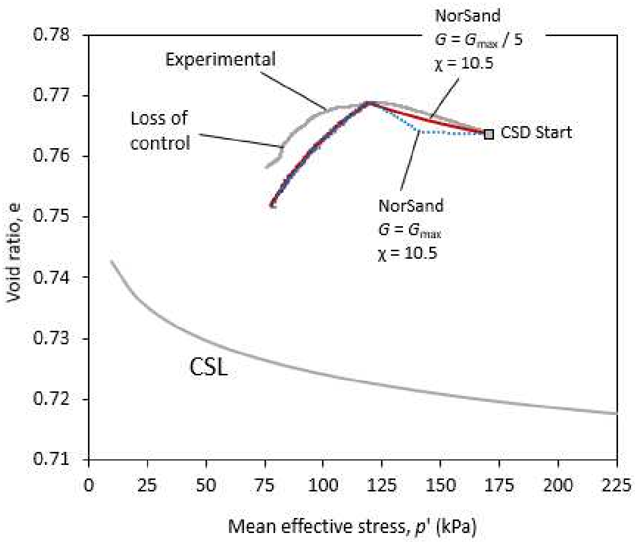

Figure 1. State diagram showing element test unloading behaviour and two simulations as part of selecting stiffness

While the modification of χ as noted produced a somewhat reasonable reproduction of the initiation of contraction seen in the experimental tests, a far too stiff behaviour was seen on the pre-yield portion of the stress path. This is reasonable given the initial adoption of G_{max} from bender elements, as clearly other forms of yielding are likely inside the idealised NorSand yield surface (e.g. Jardine 1992). To better match the "elastic" portion of the unloading path, iterative adjustment of G indicated reduction of G_{max} by a factor of five produced a reasonable match. This required reduction in G to produce matches to element tests is consistent with other recent calibrations of NorSand (Shuttle and Jefferies 2016). The element behaviour of the CSD simulation is compared to the axial and volumetric strain observed experimentally in Figure 2, showing reasonable agreement. This calibration is therefore used in all further analyses presented in the current study.

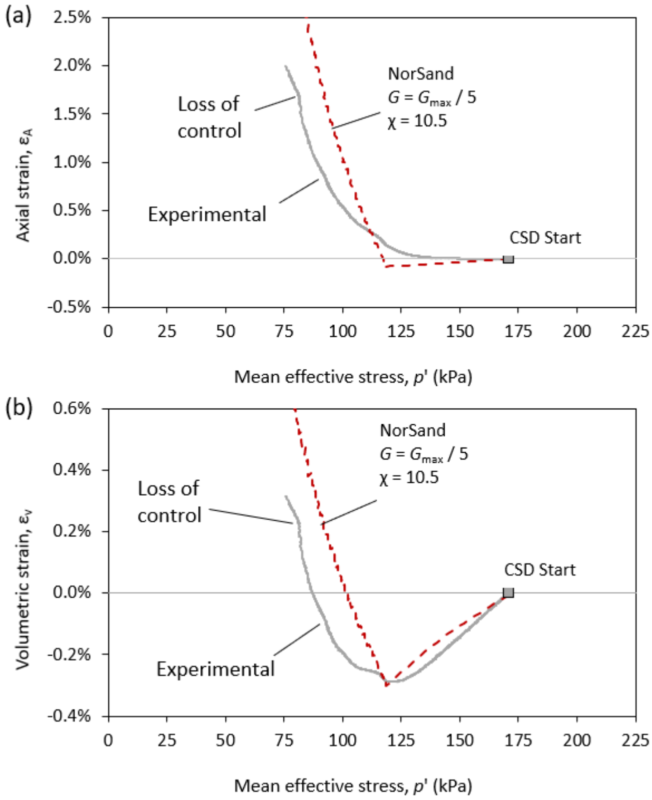

Figure 2. Comparison of numerical simulation to experimental results, (a) axial strain vs mean effective stress, and (b) volumetric strain vs mean effective stress

4 BOUNDARY VALUE PROBLEM DEVELOPMENT

The finite difference code FLAC v8.10.486 was used for the models carried out in the current paper. To enable analysis of the CSD stress path, an idealised slope geometry was developed and is presented in Figure 3. The geometry features (i) a stiff Mohr Coloumb (MC) foundation material with E'= 100 MPa, υ= 0.3, φ'=30 and c'=50 kPa, to exclude significant foundation deformations from the current examination (e.g isolating CSD effects), (ii) a starter embankment and structural zone at the perimeter of the geometry, modelled using MC, with E'= 10 MPa, υ= 0.3, φ'=35 and c'=20 kPa, (iii) the remainder of the geometry being assigned the NorSand constitutive model as per the previously-outlined calibration process. This geometry could plausibly represent a form of filtered stack or waste stockpile for sandy tailings or overburden such as that produced in many mining operations.

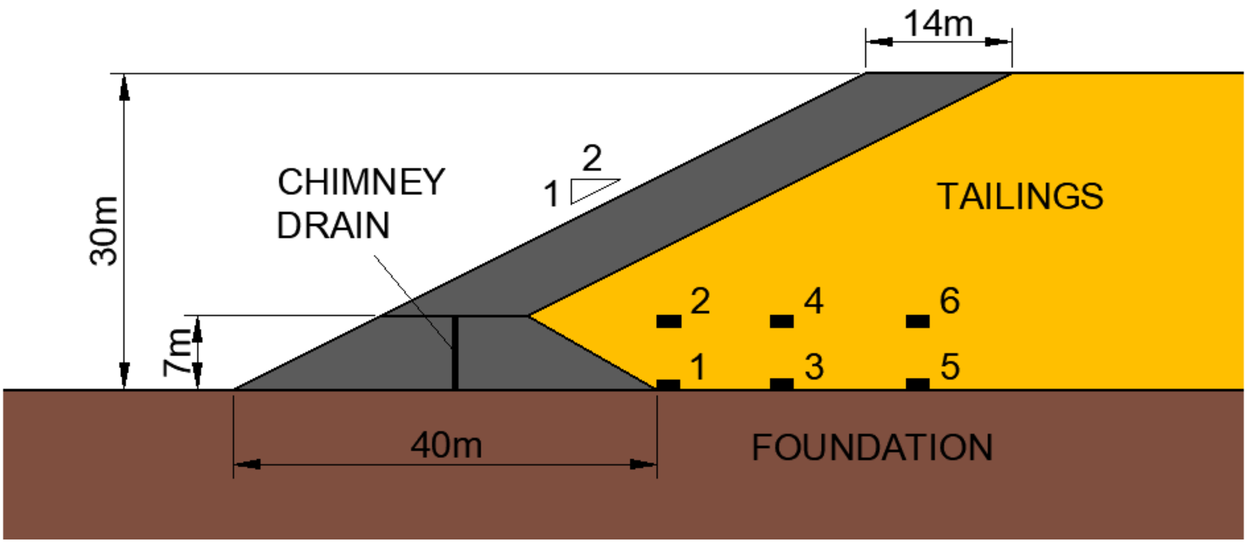

Figure 3. Geometry of idealised TSF, including locations of tracking points (1) through (6)

The tailings were initially placed in the model incrementally, with a "seed" Ψ value of +0.10 – a loose state consistent with uncompacted moist placement as common in filtered TSFs. The initial degree of saturation (S_r) of the tailings was zero, simulating a dry material for the purpose of the idealised model. The foundation was saturated with a hydrostatic pore pressure distribution during this process, with a fluid bulk modulus of zero to avoid excess pore pressure generation from tailings placement.

After placement of the tailings, the phreatic surface was increased to the tailings surface on the right boundary of the model to induce flow into the tailings – this being consistent, in a simplified manner, with ponded water near the centre of the TSF owing to poor water management. A low fluid bulk modulus of 1 kPa was adopted in this process to speed up the model run time, and as the current work is focussed on tracking the drained portion of the CSD stress path - that is, before the rapid contraction towards the CSL and initiation of instability. With a low bulk modulus selection, excess pore pressure will not be generated regardless of the rate of contraction that occurs. Finally, a zero-pore pressure condition was applied through the starter embankment, consistent with a chimney drain structure. This was applied to minimise the pore pressure values that developed on the downstream face of the starter embankment and foundation surface.

To examine the stress condition evolution below the slope during the CSD stress path, six tracking points were selected as included in Figure 3.

5 MODEL OUTCOMES

The NorSand-predicted behaviour of the six tracking points previously presented in Figure 3 are first presented in Figure 4 as a state diagram and Cambridge *p*' vs. *q* plot. From the state diagram it is evident:

- The Ψ values at the commencement of the CSD path have reduced from the initial seed value of +0.10 to a range from +0.01 to +0.02, consistent with "shear densification" below slopes with a drained increase in η – similar results with NorSand having been shown by Jefferies et al. (2019) for the Cadia TSF.
- The extent of the CSD stress path in the model developed is such that contraction towards the CSL has not yet occurred despite η values up to about 0.8. This lack of contraction appears to be a result of the shear densification and thus denser states for these below-slope elements than the seed value or element calibration test previously shown.

Turning to the behaviour of deviator stress – the primary focus of the paper, the results in Figure 5b indicate a varied response – for many of the tracking points a reduction in *q* is seen, while for others (Points 1 and 2) are fairly constant. This is an interesting outcome given the CSD stress path - by definition - being idealised as "constant". This therefore warrants further examination.

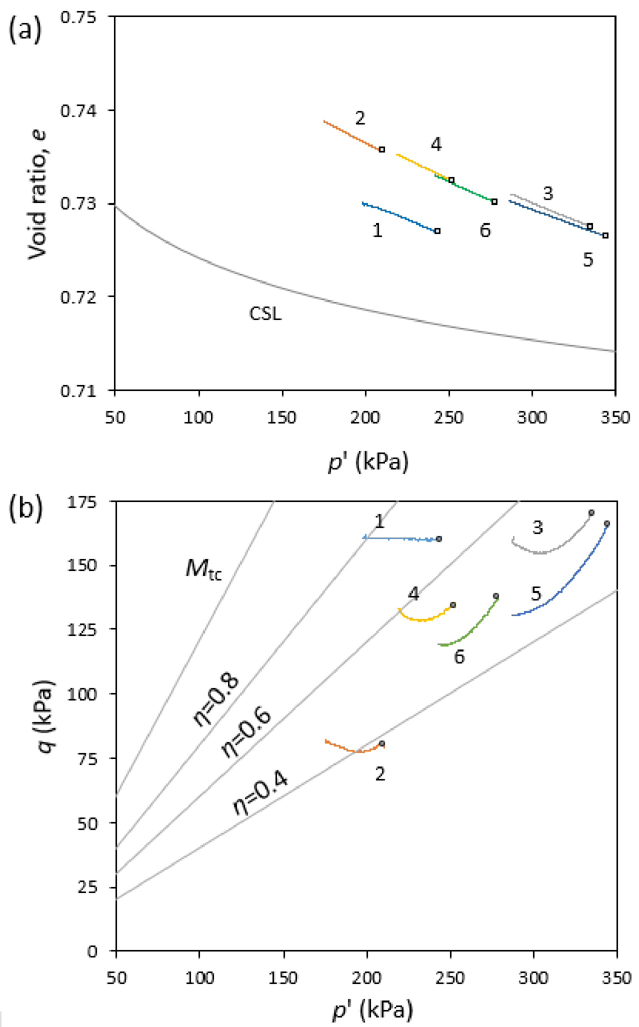

Figure 4. Observed behaviour for tracking locations during CSD process: (a) state diagram, and (b) Cambridge p' vs q plot

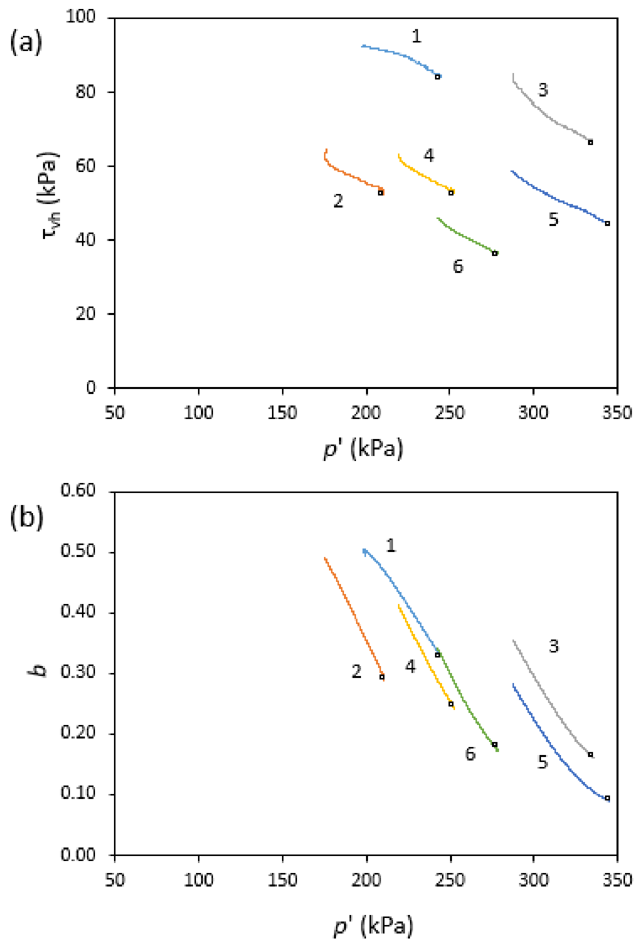

Figure 5. Observed behaviour for tracking locations during CSD process: (a) horizontal shear stress, and (b) intermediate principal stress ratio

The behaviour at the tracking points is presented in Figure 6, now as horizontal shear stress τ_{vh} and *b*. The τ_{vh} is seen to increase steadily at all points, which is a logical outcome from the increase in bulk unit weight occurring above/upstream of the tracking points with an increase in S_r. However, this might at first hand be viewed as inconsistent with the decrease in *q* discussed previously.

The evolution of *b* presented in Figure 5b provides useful insight – NorSand in plane strain conditions as used herein is seen to predict a steady and significant increase in *b*. This may have important effects, such as lowering *M* and therefore also reducing η_{IL} – commonly assumed to "scale" with *M* (Jefferies et al. 2019, Reid et al. 2022). It is noted that a tendency for *b* to increase is consistent with the plane strain compression CSD tests presented by Wanatowski et al (2010), which is to the authors' knowledge the only relevant element test program to provide comparison to the observations made here.

The observations presented for the tracking points in Figure 5 and Figure 6 have several potential implications and practical uses in slope stability and element CSD test programs:

- For element test examination of the CSD stress path, DSS programs should consider use of an increasing τ_{vh} as vertical effective stress is reduced.
- Alternatively, for stress-path type HCTS CSD programs, where all stress conditions are assigned by the tester, it appears that considering stress paths with both constant and decreasing *q* should be considered. Further, an increase in *b* during the stress path may also be appropriate.
- More broadly, the significant increase in *b* seen in the models prepared for the current work suggests lower values of *M* and η_{IL} may be relevant below slopes where a rising phreatic surface is occurring. This is an important observation when considering that triaxial compression test results are often adopted – without apparent modification – to characterise

the below-slope behaviour of tailings (Morgenstern et al, 2016, Robertson 2019).

6 CONCLUSIONS

To enable examination of the stress conditions in a BVP under a CSD stress path, an analysis of an idealised embankment using the NorSand constitutive model was carried out. The constitutive model was calibrated to element test data on SFS. The phreatic surface within an idealised embankment geometry was allowed to rise in a coupled seepage analysis with stress conditions tracked at six locations below the slope.

At the six tracking locations, an increase in τ_{vh} was seen owing to the increase in bulk unit weight from soil upstream/above the tracking points. Alternatively, a significant increase in *b* was seen at all points, along with, in some cases, a decrease in *q*. These observations are somewhat consistent with available plane strain compression CSD tests.

These observations in an idealised BVP can therefore be used to refine the test procedures used in HCTS and DSS CSD test programs, where selection of the evolution of horizontal shear stress or deviator stress are required. Cognisance of these observations may also be useful in assessing the stability of slopes within which the phreatic surface is increasing. Further modelling, plane strain element tests, and perhaps stress measurement within centrifuge models, would be useful to provide further insight and/or confirmation of these findings.

7 ACKNOWLEDGEMENTS

The authors acknowledge Dr Zhao Cheng from Itasca for providing useful insights on the inner cap implementation in FLAC.

8 REFERENCES

Alipour MJ, Lashkari A. 2018. Sand instability under constant shear drained stress path. International journal of solids and structures 150: 66–82.

Anderson SA, Riemer MF. 1995. Collapse of Saturated Soil Due to Reduction in Confinement. Journal of geotechnical engineering 121: 216–220.

Bishop AW. 1966. Sixth Rankine Lecture: The strength of soils as engineering materials. Geotechnique 16: 89–130.

Brand EW. 1985. Some thoughts on rainfall induced slope failures. Proceedings 10th International Conference on Soil Mechanics and Foundation Engineering. p. 373–376.

Chow SH, Roy A, Herduin M, Heins E, King L, Bienen B, O'Loughlin C, Gaudin C, Cassidy M. 2019. Characterisation of UWA superfine silica sand.

Chu J, Leroueil S, Leong WK. 2003. Unstable behaviour of sand and its implication for slope instability. Canadian Geotechnical Journal 40: 873–885.

Dong Q, Xu C, Cai Y, Juang H, Wang J, Yang Z, Gu C. 2016. Drained Instability in Loose Granular Material. International Journal of Geomechanics 16: 04015043.

Fanni R, Reid D, Fourie AB. 2022. Effect of principal stress direction on the instability of sand under the constant shear drained stress path. Géotechnique. Ahead of print

Gajo A. 2004. The influence of system compliance on collapse of triaxial sand samples. Canadian Geotechnical Journal 41: 257–273.

Gajo A, Piffer L, De Polo F. 2000. Analysis of certain factors affecting the unstable behaviour of saturated loose sand. Mechanics of cohesive-frictional materials 5: 215–237.

Gajo A, Wood M. 1999. Severn–Trent sand: a kinematic-hardening constitutive model: the q–p formulation. Géotechnique 49: 595–614.

Jardine RJ. 1992. Some Observations on the Kinematic Nature of Soil Stiffness. Soils and Foundations 32: 111–124.

Jefferies M. 1997. Plastic work and isotropic softening in unloading. Géotechnique 47: 1037–1042.

Jefferies M, Been K. 2015. Soil Liquefaction: A Critical State Approach, Second Edition. CRC Press.

Jefferies M, Morgenstern NR, Van Zyl DV, Wates J. 2019. Report on NTSF Embankment Failure, Cadia Valley Operations, for Ashurst Australia. .

Jefferies MG. 1993. Nor-Sand: a simle critical state model for sand. Géotechnique 43: 91–103.

di Prisco C, Imposimato S. 1997. Experimental analysis and theoretical interpretation of triaxial load controlled loose sand specimen collapses. Mechanics of Cohesive ‐ frictional Materials: An International Journal on Experiments, Modelling and Computation of Materials and Structures 2: 93‐120.

Reid D. 2020. On the effect of anisotropy on drained state liquefaction triggering. Géotechnique Letters 10: 393–397.

Reid D, Dickinson S, Mital U, Fanni R, Fourie A. 2022. On some uncertainties related to static liquefaction triggering assessments. Proceedings of the Institution of Civil Engineers - Geotechnical Engineering 175: 181–199.

Reid D, Fourie A. 2019. A direct simple shear device for static liquefaction triggering under constant shear drained loading. Géotechnique Letters 9: 142–146.

Sasitharan S, Robertson PK, Sego DC, Morgenstern NR. 1993. Collapse behavior of sand. Canadian Geotechnical Journal 30: 569–577.

Shuttle D, Jefferies M. 2016. Determining silt state from CPTu. Geotechnical Research 3: 90–118.

Skopek P, Morgenstern NR, Robertson PK, Sego DC. 1994. Collapse of dry sand. Canadian Geotechnical Journal 31: 1008–1014.

Wanatowski D. 2005. Strain softening and instability of sand under plane-strain conditions. Nanyand Technological University.

Wanatowski D, Chu J, Loke WL. 2010. Drained instability of sand in plane strain. Canadian Geotechnical Journal 47: 400–412.